Solvent-Induced Photostability of Acetylene Molecules in Clusters Probed by Multiphoton Dissociation†

Michal Fárník,* Viktoriya Poterya, and Ondřej Votava

J. Heyrovský Institute of Physical Chemistry, v.v.i., Academy of Sciences of the Czech Republic, Dolejškova 3, 182 23 Prague 8, Czech Republic

Milan Ončák and Petr Slavíček‡

Department of Physical Chemistry, Institute of Chemical Technology Prague, Technická 5, Prague 6, and J. Heyrovský Institute of Physical Chemistry, v.v.i., Academy of Sciences of the Czech Republic, Dolejškova 3, 182 23 Prague 8, Czech Republic

Ingo Dauster

Institut für Physikalische Chemie, Universität Göttingen, Tammannstrasse 6, D-37077 Göttingen, Germany

Udo Buck

Max-Planck Institut für Dynamik and Selbstorganisation, Bunsenstrasse 10, D-37073 Göttingen, Germany

Received: December 15, 2008; Revised Manuscript Received: February 5, 2009

We have studied the multiphoton photodissociation of $(C_2H_2)_n$ and $(C_2H_2)_n \cdot Ar_m$ clusters in molecular beams. The clusters were prepared in supersonic expansions under various conditions, and the corresponding mean cluster sizes were determined, for which the photodissociation at 193 nm was studied. The measured kinetic energy distributions (KEDs) of the H fragment from acetylene in clusters peak around 0.2 eV, in agreement with the KED from an isolated C_2H_2 molecule. However, the KEDs from the clusters extend to kinetic energies of over 2 eV, significantly higher than the maximum fragment energies from an isolated molecule of about 1 eV. The photofragment acceleration upon solvation is a rather unusual phenomenon. The analysis based on ab initio calculations suggests the following scenario: (i) At 193 nm, photodissociation of acetylene occurs mostly in the singlet manifold. (ii) The solvent stabilizes the acetylene molecule, preventing it from undergoing hydrogen dissociation and funneling the population into a vibrationally hot ground state. (iii) The excited C_2H_2 absorbs the next photon and eventually dissociates, yielding the H fragment with a higher kinetic energy corresponding to the first C_2H_2 excitation. Thus, the H-fragment KED extending to higher energies is a fingerprint of the cage effect and the multiphoton nature of the observed processes. The photon-flux dependence of the KEDs reflects the rate of the vibrational energy flow from the hot ground state of acetylene to the neighboring solvent molecules.

I. Introduction

Both acetylene, C_2H_2, and its photodissociation product ethynyl radical, C_2H, play important roles in combustion chemistry and soot formation. They have been implicated in some models proposed for diamond chemical vapor deposition and also in establishing the hydrocarbon balance in the atmospheres of the outer planets and their moons. From a fundamental point of view, acetylene, as one of the simplest polyatomic molecules, can be considered a prototype molecule for the passage from understanding the photochemistry of a simple diatomic to understanding the photochemistry of more complicated systems.

In this work, we investigate the effects of solvent on the photodissociation dynamics of acetylene. The solvent is represented by other acetylene molecules in $(C_2H_2)_n$ clusters and/or by rare-gas atoms in $(C_2H_2)_n \cdot Ar_m$ clusters. The profound effect of the solvent on photochemistry has been known for a long time. In 1934, Franck and Rabinowitch introduced the concept of the cage effect to explain the lowering of the yield of iodine photodissociation upon solvation.[1] More generally, the slowing of the molecular fragments and the prevention of molecular dissociation by the solvent cage are examples of molecular photostability. Photostability can be either inherent to the chromophore or induced by the solvent (as presented, for example, in this study).

Various experiments can manifest the cage effect: (i) photofragment concentration measurements, in which the photofragment yield decreases upon caging; (ii) time-domain measurements, in which the caging slows the fragmentation process; and (iii) energy-domain measurements, in which the kinetic energy of a photofragment changes as a result of interactions with the cage atoms/molecules. In the latter case, slowing of the photofragment to near-zero kinetic energies is typical evidence for pronounced caging.

Solvent effects have been studied theoretically.[2,3] Experimentally, these effects can be conveniently investigated in molecular clusters.[4,5] In our laboratory, we have witnessed

† Part of the "Robert Benny Gerber Festschrift".

* Corresponding author. E-mail: michal.farnik@jh-inst.cas.cz.

‡ E-mail: petr.slavicek@vscht.cz.

10.1021/jp811073j CCC: $40.75
Published on Web 04/15/2009

TABLE 1: Experimental Conditions for Producing $(C_2H_2)_n$ and $Ar_m(C_2H_2)_n$ Clusters and Their Corresponding Mean Sizes[a]

expanded gas	expansion pressure p_0 (bar)	nozzle temperature T_0 (K)	produced species	$\bar{n}$	$\bar{m}$
0.5% C_2H_2/Ar	2.5	253	$Ar_m(C_2H_2)_n$	5	20
1.0% C_2H_2/Ar	2.5	253	$(C_2H_2)_n$	30	—
C_2H_2	0.2	245	$(C_2H_2)_n$	≤10	—
	2.0	308	$(C_2H_2)_n$	125	—
		pickup: $Ar_m + C_2H_2$			
Ar	5.0	214	Ar_m	—	190
$p_{C_2H_2} = 0.30$ mbar			$Ar_m(C_2H_2)_n$	4	165
$p_{C_2H_2} = 0.04$ mbar			$Ar_m(C_2H_2)_n$	1	190

[a] Nozzle diameter $d = 55$ μm, length $l = 2$ mm, and opening angle $\alpha = 30°$.

solvent acting in different roles: The solvent can merely drain the energy from the photochemically active part of the system, as we have observed for hydrogen halides in rare-gas clusters.[6] The solvent can react in the ground state with the chromophore (e.g., halogen halides in water[7,8]) and in the excited state (water photochemistry[9]). The solvent can also close reaction channels by means of electronic effects (as observed in pyrrole photochemistry).[10]

The solvent effects observed for molecular clusters with acetylene are somewhat atypical. Recently, we observed that, after C_2H_2 photodissociation on a Xe_n cluster, the rare-gas Xe atoms serve as reactants in the excited state, forming rare-gas hydrides HXeCCH.[11] This type of compound was theoretically predicted and further studied by the group of Gerber.[12] Another peculiar behavior of acetylene photodissociation in clusters is presented in this contribution. The addition of solvent molecules surprisingly accelerates the molecular fragments; that is, the photofragments leaving the acetylene clusters are faster because of the cage effect than the photofragments from the direct dissociation of a single molecule. Such a phenomenon has been already observed for HI[13] and HBr clusters.[14] However, in the present case, this effect is of a different nature: the photofragment acceleration is a consequence of the acetylene photostability in the solvent and the multiphoton character of the observed process.

We show that multiphoton photodissociation represents a method for the experimental manifestation of the cage effect in molecular clusters, which relies on energy-domain measurements, but by its multiphoton nature, it is inherently connected to time-domain quantities. In a multiphoton regime, the mean time delay between the consecutive photons can be varied by changing the photon flux (i.e., the laser intensity). In a sense, the two photons can be viewed as a "pump" and a "probe". Thus, information on the duration of the molecular relaxation processes in the solvent cage can be obtained from experiments.

Before proceeding further with the photodissociation of acetylene in clusters, we briefly summarize the photodissociation of a bare C_2H_2 molecule. This topic has been addressed in numerous theoretical[15−22] and experimental[23−33] studies. The photochemistry of acetylene is dominated by hydrogen dissociation, $C_2H_2 \rightarrow C_2H + H$, with a quantum yield close to 1 at wavelengths of 193 and 121.6 nm.[30] Hydrogen dissociation can proceed via different mechanisms:[15,16] (1) In the singlet-state mechanism, after photon absorption, the acetylene molecule quickly quenches into the S_1 state. From this state, acetylene can either directly adiabatically dissociate or dissociate by a more complicated route involving internal conversion between acetylene excited states. The singlet-state mechanism is available above approximately 6.3 eV. (2) In the triplet-state mechanism, intersystem crossing between the S_1 and T_3 states[21] takes place. The triplet ground state T_1 is then quickly populated. Dissociation takes place adiabatically on the T_1 state. This mechanism seems to be operational during near-threshold acetylene photoabsorption.[29]

Yamakita et al.[34] studied the laser-induced fluorescence (LIF) and H-atom action spectroscopy of acetylene and suggested that the photodissociation mechanism changes from the triplet-mediated process to direct dissociation on the singlet-state potential energy surface (PES) at photon energies above 50600 cm^{-1} (198 nm). Zhang et al.[27] showed that, at 193 nm, the product corresponds partially to the $\tilde{A}$ state and partially to the $\tilde{X}$ state of the C_2H radical. The dominating $\tilde{X}$ state is consistent with both the triplet and singlet mechanisms, whereas molecules in the $\tilde{A}$ state appear from the singlet potential energy surface.[15,16] Photodissociation at the even shorter excitation wavelength of 121.6 nm yielded the C_2H product in the $\tilde{A}$ state exclusively.[27] The H-fragment translational energy distribution for acetylene photodissociation at 193 nm has been investigated in several groups,[24−26] and our spectra from acetylene photodissociation in clusters are compared here with those of Balko et al.[26]

This article is organized as follows: The experimental and theoretical methods are briefly outlined in the next section. Then, the experimental results are divided into the determination of the mean cluster sizes, obtained mainly from fragmentation-corrected mass spectrometric measurements, and photodissociation measurements. The results of the photolysis experiments are then discussed based on our theoretical calculations, and finally, some conclusions are drawn.

II. Methods

A. Experiments. The experimental apparatus was built and used previously at the Max-Planck Institute in Göttingen, Germany,[5,6,35,36] and moved recently to the J. Heyrovský Institute in Prague, Czech Republic.

The clusters were produced by a supersonic expansion through a conical nozzle, the parameters of which are given in Table 1. Pure acetylene and mixtures of acetylene with Ar of various concentrations were used in the expansion to produce the $(C_2H_2)_n$ and $(C_2H_2)_n \cdot Ar_m$ clusters. Alternatively, the larger Ar_m clusters were produced in pure Ar expansions and doped with C_2H_2 molecules in a pickup cell. The mean cluster sizes corresponding to the various expansion conditions are summarized in Table 1 and discussed in the following section.

After passing through a skimmer followed by two differentially pumped vacuum chambers, the second of which contained the pickup cell, the cluster beam entered a transversely mounted Wiley−McLaren time-of-flight (WMTOF) spectrometer. In the extraction region of the WMTOF spectrometer, the clusters interacted with ultraviolet (UV) photons and were photodissociated, and the H fragments were ionized and detected. The WMTOF spectrometer in the low-field mode with a small

electric field of 3−6 V cm^{-1} was used to measure the velocity distributions of the H fragments. Alternatively, the clusters could be ionized by electron impact in the subsequent vacuum chamber by a quadrupole mass spectrometer ionizer, and the mass spectra of the ionized cluster fragments could be recorded.

The acetylene was dissociated by a laser beam at 193.3 nm, generated by an ArF/F_2 excimer laser. The 25-ns-long laser pulses at a 10-Hz repetition rate were focused by a 366-mm LiF lens to a spot of about 10^{-4} cm^2 at the intersection with the molecular beam. The maximum energy at the interaction region was about 40 mJ, corresponding to a photon flux of about 10^{28} cm^{-2} s^{-1}. The laser beam intensity was varied in order to distinguish the multiphoton processes.

The arising H fragments were efficiently ionized at 243.07 nm through one-color resonance-enhanced multiphoton ionization (REMPI) in the 2 + 1 excitation scheme. The ionization wavelength was generated by mixing the fundamental 1064-nm output of a Nd:YAG laser with the frequency-doubled output of a dye laser pumped by the second harmonic of the Nd:YAG laser and operated at 630.3 nm. The system produced laser pulses of 5-ns duration, and the energy employed in the present experiments was 0.7 mJ/pulse in the interaction region. The laser beam was focused into the vacuum chamber with a 400-mm quartz lens onto a 14-μm spot (Gaussian beam waist). The tight focus resulted in high photon fluxes of approximately 10^{28} cm^{-2} s^{-1} comparable to the maximum 193-nm photon fluxes.

The laser pulses were synchronized using a pulse delay generator so that the 193-nm pulses preceded the 243-nm pulses by 5−10 ns. The spatial overlap of the two laser beams and the molecular beam was adjusted on the maximum signal and a symmetric shape of the H-fragment spectrum from the well-studied $(HBr)_n$ test system.[4]

In the data analysis process, the measured TOF spectrum was converted to the kinetic energy distribution (KED) of the fragment H atoms. The analysis involved a complete Monte Carlo (MC) simulation of the particle trajectories, which was carried out considering the molecular beam data, the photodissociation process parameters, the WMTOF geometry, the finite interaction volume, and the detector electronic response.[4]

B. Ab Initio Calculations. The photochemistry of the acetylene molecule was further investigated by tools of quantum chemistry. We calculated cuts through the potential energy surfaces of both the isolated acetylene molecule and the C_2H_2·Ar dimer. The latter complex served as a model for the exploration of solvent effects on acetylene photochemistry. All local minima in the acetylene potential energy surface were calculated at the multireference configuration interaction (MRCI) level, with an active space of eight electrons in eight orbitals [henceforth denoted as (8,8)] and two and seven core orbitals for the C_2H_2 and the C_2H_2·Ar systems, respectively. Transition states were optimized at the CASSCF(8,8) level. Three states were averaged for calculations of the singlet surface; for triplet calculations, three singlet and three triplet states were averaged in the CASSCF calculations. Local minima and transition states were located by standard algorithms as implemented in the Molpro program package. A frequency analysis was performed to confirm the character of the stationary points. Isomers with dissociated hydrogen atoms were modeled as partially optimized structures with a constrained C—H distance of 3.5 Å. Conical intersections (CIs) of S_2/S_1 and S_1/S_0 states were localized by constrained optimization on the upper electronic state at the CASSCF(8,8) level; structures of the S_0/T_1 and S_1/T_3 crossing points were taken from the literature. These were then used as starting geometries for numerical searches at the MRCI(8,8) level. We used a 6-31+g* basis set for C and H atoms and a 6-31g basis set for argon. Although no symmetry constraints were applied in the calculations, all stationary points exhibited C_s symmetry.

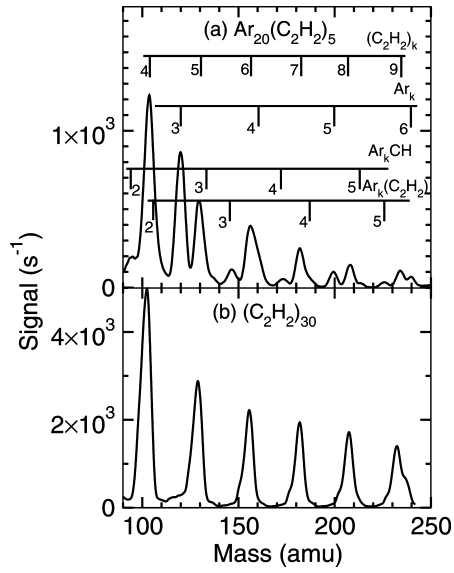

Figure 1. Mass spectra of acetylene clusters generated in supersonic expansion of an acetylene/Ar mixture at 2.5 bar and 253 K: (a) 0.5% C_2H_2/Ar corresponding to mixed $Ar_m(C_2H_2)_n$ clusters with a mean cluster size of $\bar{m} = 20$, $\bar{n} = 5$; (b) 1.0% C_2H_2/Ar, corresponding to pure $(C_2H_2)_n$ clusters with a mean cluster size of $\bar{n} = 30$. The top scales indicate the positions of the $(C_2H_2)_k^+$, Ar_k^+, Ar_kCH^+, and $Ar_kC_2H_2^+$ series of mass peaks.

The scans through the potential energy surface were performed at the MRCI(8,8) level. Linear interpolations between different points on the acetylene potential energy surface were performed in the internal coordinates. We also carried out the same scans for the C_2H_2·Ar complex, with the argon atom fixed at a distance of 4 Å from carbon bonded to the dissociating hydrogen atom. The C—C—Ar angle was set equal to the C—C—H angle + 20°. We note that this arrangement was chosen to represent the basic features of solvation, although it does not reflect the correct minimum position.

All calculations were performed in the Molpro package.[37]

III. Results

A. Cluster Size Distributions. In this section, we discuss the techniques used to produce the clusters and determine the mean cluster sizes generated under the various expansion conditions. In particular, we used three different approaches for cluster formation: expansions of (i) C_2H_2/Ar mixed gases and (ii) of pure C_2H_2 and (iii) the pickup of C_2H_2 on Ar_n clusters. The selected expansion conditions and the corresponding cluster sizes are summarized in Table 1. Generally, the cluster size distributions of the larger clusters can be characterized by log-normal distributions of a width comparable to the mean size.[38]

Electron-impact ionization of the cluster beam and subsequent quadrupole mass spectrometry was utilized to yield insight into the cluster size distribution and composition. Figure 1 shows such mass spectra for acetylene clusters generated in supersonic expansions of acetylene/Ar mixtures at 2.5 bar and 253 K. The top spectrum (a) corresponds to the expansion of a 0.5% C_2H_2/Ar mixture, and the bottom one (b) corresponds to the expansion of a 1% mixture. The positions of the $(C_2H_2)_k^+$, Ar_k^+, Ar_kCH^+, and $Ar_kC_2H_2^+$ mass peaks are indicated. Whereas the bottom spectrum is clearly dominated by the $(C_2H_2)_k^+$ ions, the top

spectrum also exhibits peaks corresponding to the Ar_kCH^+ and $Ar_kC_2H_2^+$ fragments, suggesting the production of mixed $(C_2H_2)_nAr_m$ clusters in the expansion. There is also a strong contribution of Ar_k^+ ions in this spectrum.

To determine the relation between those measured fragment masses and the original neutral cluster sizes, we refer to an analogy with $(HBr)_n$. For the latter clusters, a detailed scattering experiment was performed on the present experimental apparatus in Buck's group,[35] which provided independent measurements of the neutral cluster size distributions prior to electron-impact ionization. Such an analogy is reasonable, given that the interaction energies in acetylene clusters are similar to those in HBr clusters; for example, the binding energies of both $(C_2H_2)_2$[39] and $(HBr)_2$[40] dimers are approximately 60 meV. By extrapolation of the $(HBr)_n$ fragmentation data[35] and comparison with the present mass spectra, we obtained the mean neutral cluster size $\bar{n} \approx 30$ for the $(C_2H_2)_n$ clusters under the present experimental conditions of 2.5 bar and 253 K.

In principle, mixed $Ar_m(C_2H_2)_n$ clusters can be prepared by the expansion of C_2H_2/Ar mixtures. Considering the binding energy of an acetylene molecule of ~120 meV in the larger $(C_2H_2)_n$ clusters (it generates two T-shaped bonds) and the binding energy of an Ar atom in an Ar_m cluster of about 12 meV, the energy released upon generation of the $(C_2H_2)_{30}$ cluster would be sufficient to evaporate about 285 Ar atoms. This value far exceeds the mean Ar_m cluster size of $\bar{m} = 55$ that is generated by the pure Ar expansion at the above conditions of 2.5 bar and 253 K. Therefore, all of the Ar atoms can be evaporated during the clustering process, and bare $(C_2H_2)_n$ clusters with $\bar{n} \approx 30$ are generated in the 1% mixture expansion under these conditions (even if a somewhat higher binding energy between acetylene molecule and Ar atom is considered). This conclusion is supported by the mass spectra composed of only the $(C_2H_2)_k^+$ mass peaks.

In contrast, the spectrum in Figure 1a exhibits both Ar_kCH^+ and $Ar_kC_2H_2^+$ fragments, suggesting the production of mixed $Ar_m(C_2H_2)_n$ clusters. In analogy to the above analysis, we obtained a mean neutral $(C_2H_2)_n$ cluster size of $\bar{n} \approx 5$. This would yield the evaporation of 35 atoms from the Ar_m cluster with $\bar{m} = 55$, and this, in turn, would result in the generation of $Ar_m(C_2H_2)_n$ clusters with $\bar{n} = 5$ and $\bar{m} = 20$ in the expansion of the 0.5% mixture under the same conditions.

Figure 2 shows the mass spectra of clusters generated by a pickup process of acetylene molecules on Ar clusters produced in supersonic expansions at 5.0 bar and 214 K. The mean cluster size of the pure Ar_m clusters produced in the expansion under these conditions gives $\bar{m} = 190$. The top spectrum (a) corresponds to an acetylene pressure in the pickup cell of 0.3 mbar and is clearly dominated by the series of $(C_2H_2)_k^+$ mass peaks. This suggests that several acetylene molecules are embedded in the Ar_m cluster and coagulate to generate $(C_2H_2)_n$ clusters. The mean cluster size of $\bar{n} \approx 4$ was evaluated as above from the mass spectra. The generation of a $(C_2H_2)_4$ cluster releases an energy sufficient to evaporate about 25 Ar atoms from the cluster; therefore, the final cluster composition will be $Ar_m(C_2H_2)_n$ with $\bar{m} = 165$ and $\bar{n} = 4$.

On the other hand, the bottom spectrum in Figure 2b, recorded at a lower pickup pressure of 0.04 mbar, is dominated by the Ar_k^+ mass peak series, accompanied by Ar_kCH^+ and $Ar_kC_2H_2^+$ mass peaks. A careful analysis and comparison of the various spectra measured at different pickup pressures suggests that $(C_2H_2)_k^+$ mass peaks are not present in the spectra at this low acetylene pressure. This, in turn, indicates the presence of a single molecule on the Ar cluster, that is, $Ar_mC_2H_2$ species with

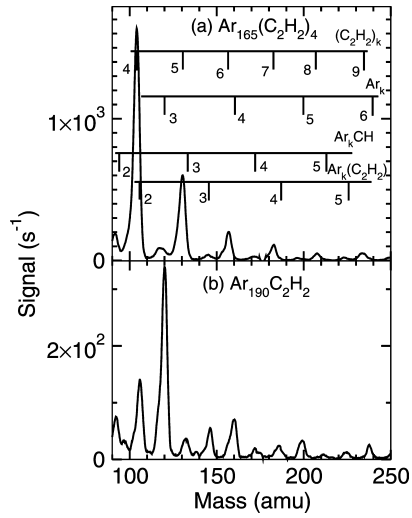

Figure 2. Mass spectra of clusters generated by a pickup process of C_2H_2 molecules on Ar clusters produced in supersonic expansion at 5.0 bar and 214 K for various acetylene pressures in the pickup cell: (a) 0.3 mbar, which corresponds to the generation of $Ar_m(C_2H_2)_n$ clusters with a mean cluster size of $\bar{m} = 165$, $\bar{n} = 4$; (b) 0.04 mbar, which corresponds, on average, to the pickup of only a single acetylene molecule, i.e., $Ar_mC_2H_2$, $\bar{m} = 190$. The top scales indicate the positions of the $(C_2H_2)_k^+$, Ar_k^+, Ar_kCH^+, and $Ar_kC_2H_2^+$ series of mass peaks.

$\bar{m} = 190$. Given that, for a pickup pressure of 0.3 mbar, a pickup of about four acetylene molecules has been derived, it is consistent that, at pressures more than 5 times lower, the average number of embedded molecules is $\bar{n} \leq 1$. It is also worth noting that, in earlier pickup experiments on our apparatus with HBr molecules on Ar clusters of similar sizes,[14,41] the pickup of a single HBr molecule was also derived for a pickup pressure of 0.04 mbar, in excellent agreement with the present value.

To ensure the production of pure $(C_2H_2)_n$ clusters, pure acetylene expansions were again exploited. Because the clusters produced by this method were generally too large for the mass range of our mass spectrometer, their cluster sizes were calculated approximately. Bobbert et al.[38] measured reliable size distributions of large neutral ammonia and water clusters, which were analyzed in terms of a modified scaling law of the Hagena type.[42] A similar formula was employed here to obtain the mean cluster size

$$\bar{n} = D(\Gamma^*/1000)^a, \quad \Gamma^* = n_0 d_a^{\,q} T_0^{\,q-3}/K_c \qquad (1)$$

where $d_a = 0.933d/tg(\alpha/2)$ is the equivalent nozzle diameter of a conical nozzle with a smaller diameter d and cone angle α. The parameters $D = 33.02$, $a = 1.348$, and $q = 0.659$ were taken from the fit to the experimental ammonia cluster sizes.[38] The characteristic parameter K_c was obtained as $K_c = (r_cT_c)^{q-3}$, where $r_c = 3.90$ Å was determined from the acetylene density ρ and molecular mass m as $r_c = (m/\rho)^{1/3}$ and $T_c = 2780$ K corresponds to the latent heat of vaporization as $kT_c = \Delta h = 23.1$ kJ/mol.[43]

Using the above formulas for the typical expansion conditions of 2.0 bar and 308 K, the mean cluster size corresponds to $\bar{n} = 125$. For small clusters, the application of this formula becomes questionable. For 0.2 bar and 245 K, the equation would yield $\bar{n} \approx 11$. Nevertheless, the value $\bar{n} \leq 10$ is indicated in Table 1, because only fragments significantly smaller than $(C_2H_2)_{10}^+$ were observed in the measured cluster fragment mass spectra, yet at the same time, there still is a clear evidence for some cluster species under those conditions.

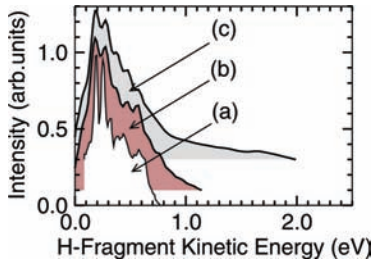

Figure 3. H-fragment KED from the photodissociation of acetylene at 193 nm: (a) spectrum of the C_2H_2 molecule from the literature[26] for comparison (photon flux $N_{ph} \leq 10^{26}$ cm^{-2} s^{-1}), (b) spectrum measured with C_2H_2 molecules diffused into the laser interaction region ($N_{ph} = 1.6 \times 10^{28}$ cm^{-2} s^{-1}), and (c) spectrum obtained in a molecular beam containing small $(C_2H_2)_n$ clusters with a mean cluster size of $\bar{n} \leq 10$ ($N_{ph} = 7 \times 10^{26}$ cm^{-2} s^{-1}).

B. Cluster Photodissociation. In this section, we present the results of the photodissociation of acetylene molecules in clusters. First, a comparison with the photodissociation of a bare C_2H_2 molecule is provided in Figure 3, where the bottom trace (a) shows the H-fragment KED from photodissociation of an acetylene molecule at 193 nm from the literature.[26] The middle trace (b) shows the KED measured in our experiments with bare C_2H_2 molecules diffused from the pickup cell in the neighboring vacuum chamber into the laser interaction region. Our spectrum exhibits a somewhat lower resolution. More importantly, whereas the C_2H_2 molecule KED (trace a) extends to a maximum energy of about 0.7 eV, our spectrum exhibits a contribution from faster H fragments with energies up to approximately 1.1 eV. This is due to the secondary photodissociation process of the ethynyl radical

$$C_2H_2 \xrightarrow{h\nu} H + C_2H \xrightarrow{h\nu} H + C_2 \qquad (2)$$

which was also observed previously by Balko et al.[26] They reported a significant fraction of the detected H atoms originating from the secondary dissociation at moderate laser powers above 10^{26} cm^{-2} s^{-1}. The present photon flux was much higher, $N_{ph} = 1.6 \times 10^{28}$ cm^{-2} s^{-1}, so secondary processes are likely to occur.[44]

The top trace (c) shows the measurements for a beam of $(C_2H_2)_n$ clusters with a mean cluster size of $\bar{n} \leq 10$. Clearly, a much longer tail of KED with H-fragment energies up to approximately 2 eV is observed. The generation of these fast fragments results from secondary photodissociation in clusters as discussed below. The photon flux corresponding to spectrum c was a factor of about 20 lower than that for spectrum b, $N_{ph} = 7 \times 10^{26}$ cm^{-2} s^{-1}, yet secondary processes were still observed.

The effect of the laser power on the H-fragment KED is further illustrated for larger $(C_2H_2)_n$ clusters with a mean cluster size of $\bar{n} = 125$ in Figure 4. The solid and dashed lines show the KEDs measured at the photon fluxes of $N_{ph} = 1.5 \times 10^{28}$ cm^{-2} s^{-1} and 1.7×10^{27} cm^{-2} s^{-1}, respectively. Again, under both experimental conditions, secondary processes are possible. Although the low-kinetic-energy parts of the two spectra are almost identical (the spectra were normalized on the maximum for comparison), there is a significantly higher portion of the faster fragments for the higher photon flux, suggesting that these fragments result from some secondary process generated by subsequent photon (or photons) interacting with the cluster. Similar dependencies have been measured for other cluster sizes as well.

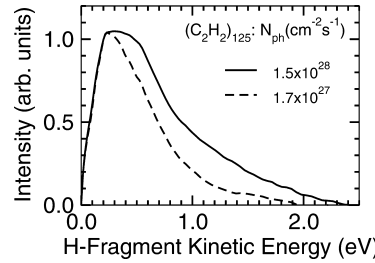

Figure 4. Dependence of the H-fragment KED from the 193-nm photodissociation of $(C_2H_2)_n$, $\bar{n} = 125$, clusters on laser photon flux: $N_{ph} = 1.5 \times 10^{28}$ cm^{-2} s^{-1} (solid line) and $N_{ph} = 1.7 \times 10^{27}$ cm^{-2} s^{-1} (dashed line).

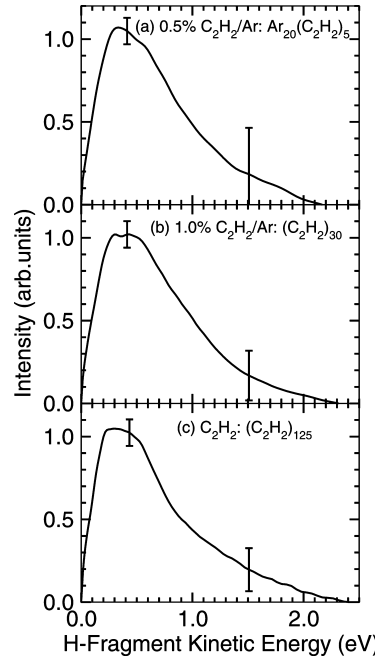

Figure 5. H-fragment KEDs from the 193-nm photodissociation of acetylene clusters generated under various expansion conditions: (a) 0.5% C_2H_2/Ar mixture at 2.5 bar and 253 K, corresponding to mixed $Ar_m(C_2H_2)_n$ clusters with a mean cluster size of $\bar{m} = 20$, $\bar{n} = 5$; (b) 1.0% C_2H_2/Ar at 2.5 bar and 253 K corresponding to pure $(C_2H_2)_n$ clusters with a mean cluster size of $\bar{n} = 30$, and (c) pure acetylene expansion corresponding to $(C_2H_2)_n$, $\bar{n} = 125$. The estimated error bars of the KEDs are indicated in the regions of low and high fragment kinetic energy.

Figure 5 shows the H-fragment KEDs from clusters generated under various expansion conditions discussed in the previous section: (a) 0.5% C_2H_2/Ar mixture at 2.5 bar and 253 K corresponding to mixed $Ar_m(C_2H_2)_n$, $\bar{m} = 20$, $\bar{n} = 5$, clusters; (b) 1.0% C_2H_2/Ar at 2.5 bar and 253 K corresponding to pure $(C_2H_2)_n$, $\bar{n} = 30$, clusters; and (c) pure acetylene expansion corresponding to $(C_2H_2)_n$, $\bar{n} = 125$. Similar KEDs were also obtained for other cluster sizes and expansion conditions. There seems to be no really significant effect of the cluster size or composition on the photodissociation dynamics of acetylene molecules in clusters in the investigated size and composition range. The most striking difference of these spectra compared to the single-molecule spectrum in Figure 3a is the long tail of the faster fragments extending to about 2.2 eV.

Qualitatively, somewhat different TOF spectra were obtained for the photodissociation of clusters generated by the pickup process of acetylene on Ar_m clusters, which is illustrated in Figure 6. Here, the measured TOF spectra are shown rather than the KEDs, because the differences are mainly observed for the

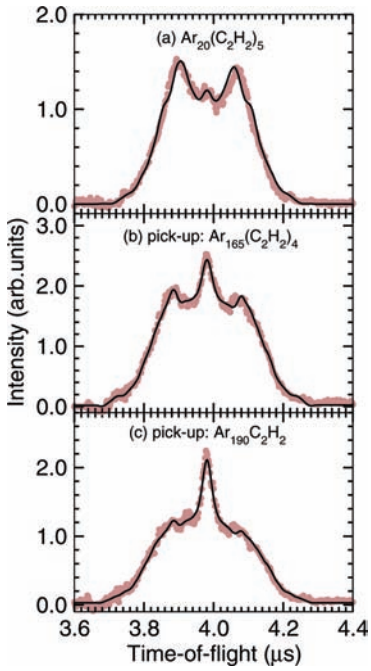

Figure 6. H-fragment TOF spectra from the 193-nm photolysis of various mixed $Ar_m(C_2H_2)_n$ clusters: (a) clusters generated in the expansion of a 0.5% C_2H_2/Ar mixture at 2.5 bar and 253 K, corresponding to a mean cluster size of $\bar{m} = 20$, $\bar{n} = 5$; (b) clusters with $\bar{m} = 165$, $\bar{n} = 4$ generated by the pickup process on Ar_{190} clusters; and (c) $Ar_{190}C_2H_2$ clusters with a single acetylene molecule.

near-zero-kinetic-energy fragment region, which is more pronounced in the TOF spectra.[46] The zero-kinetic-energy fragments peak in the middle of the TOF spectra at around 3.89 μs. There is only a small increase in intensity in this region in the spectrum of $Ar_{20}(C_2H_2)_5$ clusters generated in 0.5% C_2H_2/Ar mixture expansion (trace a) (from this spectrum, the KED in Figure 5 has been obtained). On the other hand, this peak becomes the maximum of the TOF spectrum for the $Ar_{165}(C_2H_2)_4$ clusters (trace b) produced in the pickup process, and its relative intensity even increases for the $Ar_{190}C_2H_2$ clusters (trace c).

IV. Discussion

The surprising outcome of the present study is that, upon solvation, faster hydrogen fragments appear. This contradicts the usual manifestation of the cage effect, specifically, the slowing of the molecular fragments. We already showed above that multiphoton processes have to be considered for the interpretation of these results (see the discussion of Figures 3 and 4 in the previous section). Although the secondary photodissociation of C_2H can yield some faster H fragments with energies up to about 1.1 eV,[26] it cannot produce the observed H fragments with significantly higher kinetic energies of up to about 2.2 eV. It ought to be mentioned that the high-energy H fragments with energies above approximately 1 eV are produced only in the clusters. Therefore, the nature of the multiphoton processes in the clusters must be quite different.

It should also be mentioned that the H atoms produced deep inside the cluster interior can recombine with C_2H. This process favors the slow H fragments, which then cannot escape from the cluster. Therefore, the escaping H atoms are biased toward higher kinetic energies. Nevertheless, the observed KED with fragments significantly faster than the fragments from C_2H_2 molecules cannot be explained merely by depletion of the slow hydrogen atoms. In addition, the significantly faster H fragments

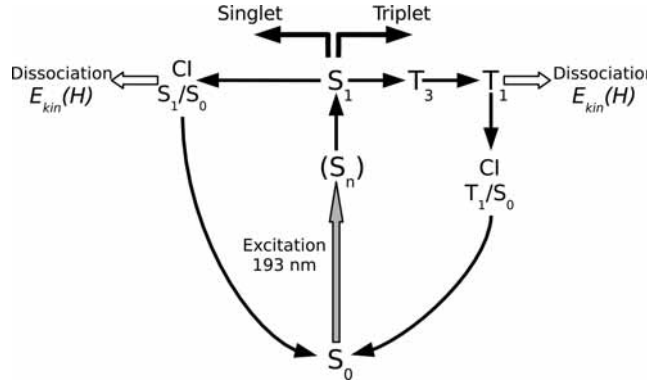

Figure 7. Possible photochemical pathways of the acetylene molecule upon absorption of 193-nm photons.

are observed also in Ar clusters with a single C_2H_2 molecule, where recombination cannot occur.

If we consider multiphoton processes, it is possible to explain the appearance of the faster hydrogen fragments as a consequence of acetylene photostability: After the first photon is absorbed, acetylene quenches in the cluster environment into a hot ground state and subsequently dissociates from this state upon absorption of the second photon. The hot ground state lies higher in energy, and therefore, the fragments acquire higher translational energy. The time delay between the two consecutive photons is long enough to allow for all necessary dynamical processes to take place.[47] Furthermore, the average time delay between a pair of photons can be varied by changing the photon intensity.

In addition to multiphoton processes, the possibility of dissociating more than one molecule within the cluster has to be considered. Taking into account the high photon fluxes mentioned above (see also the comment regarding secondary processes[44]), up to about 50 C_2H_2 molecules can be dissociated within the laser pulse at the highest laser powers used here. This could lead to the complete dissociation of all of the molecules in the smaller clusters. The cluster probably decays during such massive dissociation. The H fragments photolyzed from the molecules already freed from the cluster would contribute to the molecule-like spectrum. On the other hand, the H atoms photolyzed from those molecules that are still at least partly solvated and thus eventually quenched by the cluster would contribute to the high-energy tail. Thus, both contributions expected for multiphoton single-molecule dissociation in the cluster would be present. The question might arise as to how the ratio of these contributions in the KED would be changed by the photolysis of many molecules. Massive cluster decay would probably give rise to a larger contribution from the freed molecules at higher rather than lower photon flux, so that more slow fragments below 1 eV should be generated at the higher photon flux. However, the experimental evidence shown by the KEDs in Figure 4 suggests just the opposite: the KED measured at higher photon flux exhibits more faster fragments. Thus, the photolysis of more than one molecule in the cluster cannot be excluded but is not expected to significantly influence the conclusions drawn below.

Figure 7 schematically depicts processes following photon absorption by an acetylene molecule. The molecule is promoted into either the first or higher excited singlet state (in the latter case, it immediately relaxes into the first excited S_1 state). The dissociation can proceed either directly on the singlet state potential energy surface (with nonadiabatic transitions between S_1 and S_2 state playing a role) or via intersystem crossing (ISC)

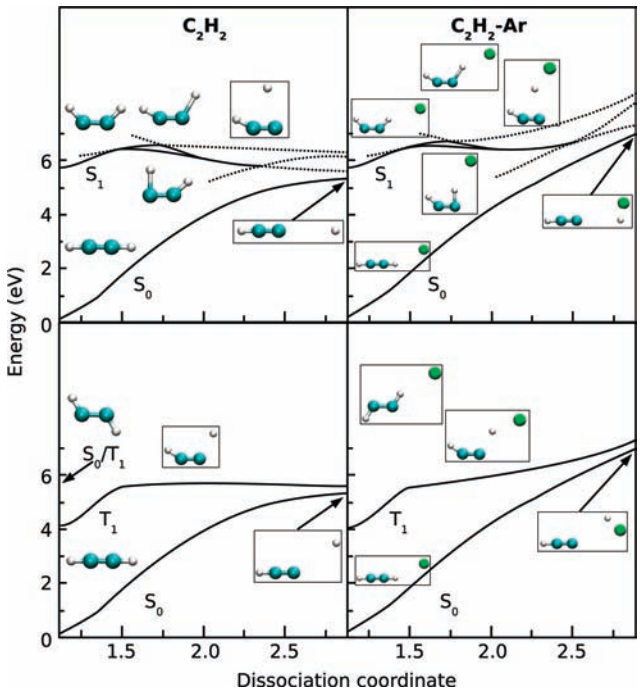

Figure 8. Potential energy curves for acetylene photodissociation calculated at the MRCI(8,8)/6-31+g* level of theory. Processes in the lowest excited singlet state and lowest triplet state are considered; the ground-state potential energy curve is also included. The important structures depicted in the figure were optimized at the MRCI(8,8)/6-31+g* (local minima) and CASSCF(8,8)/6-31+g* (transition states) levels, and geometries connecting these structures were acquired by linear interpolation. Solid lines represent energies calculated at geometries optimized (with a constrained C—H distance) for a given electronic state or interpolations between such points. Energies calculated at extrapolated geometries are depicted by dotted lines. On the left side of the figure, curves for isolated acetylene are depicted; in the right panel, an Ar atom is added to mimic the solvent effects (see also section II.B).

to the T_3 state with subsequent internal conversion to the T_1 state and adiabatic dissociation from this state. Both mechanisms are consistent with the experimentally observed features of the KED spectrum:[26] a maximum at approximately 0.2 eV and extension of the curve up to 0.8 eV. In the triplet mechanism, the maximum would correspond to the difference between the dissociation transition-state energy and the $\tilde{X}^2\Sigma$ asymptote of the C_2H product; for the singlet-state pathway, the energy maximum of 0.2 eV would correspond to the $\tilde{A}^2\Pi$ asymptote of the C_2H fragment.

It is easy to imagine that the rates of both of these dissociation channels (singlet and triplet) will be slowed significantly in the presence of a solvent. The solvent effect on acetylene photodissociation is visualized in Figure 8. The linear interpolation curves calculated at the MRCI(8,8)/6-31+g* level are shown for both the singlet and triplet mechanisms. The solvent molecule is represented by an argon atom as described in section II.B. It can be seen that the solvent atom does not significantly affect the reaction barriers for dissociation. However, it prevents the hydrogen from leaving the molecule. For the triplet mechanism, this means preserving the molecule in the lowest triplet state, whereas for the singlet mechanism, the solvent induces quenching into the ground singlet electronic state. Note also that the solvent does not significantly change the energy of the S_1/S_0 conical intersection; this is very different than for the photodissociation of the pyrrole molecule, for example, where the solvent completely removes the conical intersection, switching off the whole reaction channel.[10,48]

We stated above that the hydrogen KED does not provide the complete information necessary to distinguish between the singlet and triplet photodissociation mechanisms. Here, we argue that, at 193 nm, the singlet mechanism is more probable. Even the lowest triplet state lies about 4 eV above the Franck—Condon point of the bare acetylene molecule. Thus, photodissociation of the C_2H_2 molecule from this state with the second 193-nm photon should yield fast H fragments with up to 5 eV of excess kinetic energy (considering fast internal relaxation in the triplet manifold). We see no evidence for such fast fragments in our spectra, however. Therefore, we infer a quenching of the excited molecule into a vibrationally hot ground state S_0. As is seen in Figure 8, such a relaxation is easily possible on the singlet surface. Figure 8 also shows how the solvent funnels the electronic population into the ground electronic state. Note, at this point, that there is also an energetically accessible crossing between T_1 and S_0 states. However, we do not expect T_1/S_0 ISC to play a major role because the spin—orbit coupling between these states is rather low (about 1 cm^{-1}) and the crossing is not entropically favored on the T_1 potential energy surface.

Our suggestion that the acetylene photodissociation mechanism is dominated at 193 nm by the singlet-state mechanism and that the acetylene molecule in a confined environment quenches to the ground state via an internal conversion process is consistent with the experiments performed by Yamakita et al.[34] In their work, evidence was provided that the photodissociation mechanism changes from the triplet-mediated dissociation to the direct dissociation on the PES of the $\tilde{A}$ state at about 198 nm.

It should be considered that also the 243-nm photons used for H-atom REMPI detection might contribute to the photodissociation of the vibrationally excited C_2H_2 molecules in the cluster, given that the photon fluxes at 243 nm were comparable to those at 193 nm. The photodissociation of vibrationally excited C_2H_2 molecules has been investigated by Ganot et al.[31] In their work, acetylene molecules were prepared in rovibrational states in the region of three C—H stretch quanta and photodissociated with 243-nm photons. A similar mechanism can occur in our experiments as well. The first 193-nm photon promotes the C_2H_2 molecule into the S_1 excited state, which is quenched by the cluster to vibrationally excited S_0, and then a 243-nm photon can dissociate the molecule. However, in our experiments, we cannot distinguish whether the secondary dissociating photon has a wavelength of 193 or 243 nm.

At this point, it is meaningful to discuss Figure 4 in the context of the above-proposed mechanism. This figure shows the H-fragment KEDs from the photodissociation of $(C_2H_2)_n$, $\bar{n} = 125$, clusters at two different photon fluxes. Both KEDs exhibit the high-energy-fragment tail due to the secondary photodissociation of the excited C_2H_2 molecules. However, this tail is significantly suppressed in the KED measured at the lower laser power. Actually, this measurement in the energy domain provides some information about the quenching dynamics of the excited C_2H_2 molecule and its subsequent cooling in the cluster in the time domain as schematically illustrated in Figure 9. Using the C_2H_2 molecule absorption cross section $\sigma = 1.347 \times 10^{-19}$ cm^{-2},[45] the photon flux of 1.5×10^{28} cm^{-2} s^{-1} can be roughly converted into a mean time delay of 0.5 ns between two successive photons absorbed by the molecule. On the other hand, the lower photon flux results in a mean time delay of about 5 ns. Therefore, in the latter case, the molecule in the cluster has, on average, 10 times as long to dissipate the excess energy to the cluster in the vibrational ground state of S_0. The

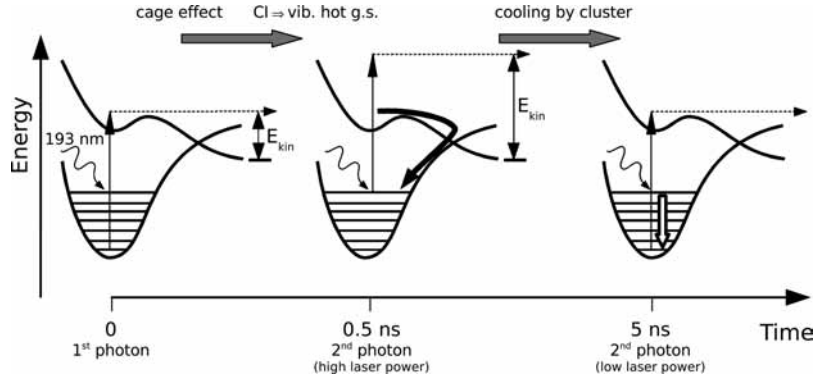

Figure 9. Schematic picture of multiphoton dissociation, providing time-domain information about the cage effect by the energy-domain measurements. At time zero, the molecule is excited; subsequently, the cage effect quenches the molecule into the vibrationally hot ground state, and a second photon dissociates the molecule from this state, resulting in fragments with a higher kinetic energy. If the second photon time delay is longer, the molecule is further cooled by the cluster into lower vibrational states from which slower fragments originate upon photodissociation.

spectra suggest that, 0.5 ns after excitation, some C_2H_2 molecules in the cluster are still vibrationally hot and yield fast H fragments. After 5 ns, significantly fewer C_2H_2 molecules are still in the vibrationally excited state. Nevertheless, even then, some molecules are not fully vibrationally relaxed. It has been established by vibrational predissociation studies of small complexes that energy flow time scales are typically in the range from 0.1 to 100 ns,[49] consistent with the present observations. Thus, the present energy-domain measurements provide some information about the cage effect and excitation energy dissipation within the cluster in the time domain. It should be stressed that the real explicit time-domain information can be obtained only from a state-of-the-art pump−probe experiment (see, e.g., refs 50 and 51). It would be nice to investigate the present dynamics in a real time-resolved experiment, which is, however, beyond our present experimental capabilities.

Other less-probable possibilities for explaining the appearance of the fast hydrogen fragments in the multiphoton photodissociation of acetylene clusters should be also discussed. One could, for example, consider the possibility of reactions between acetylene molecules. Also, one could think of a mechanism in which departing H atoms from one molecule could vibrationally excite a neighboring molecule, as was suggested for HBr clusters.[14] This is, however, an improbable mechanism for energy reasons. Because most of the departing hydrogen atoms have low energies (0.2 eV), additional excess energy of more than 1 eV cannot be explained in this way. In addition, fast H fragments were observed even in Ar clusters with a single C_2H_2 molecule.

Similarly, faster H fragments have also been observed in the photodissociation of small HI clusters.[13] The fast H atoms originate from superelastic scattering from spin−orbit-excited $I(^2P_{1/2})$ fragments of primary photodissociation. This mechanism, however, requires a relatively strong spin−orbit coupling, which is 0.94 eV for iodine but more than 2 orders of magnitude weaker for carbon. Thus, such a process will not affect the energetics in our system significantly. Indeed, the C_2H fragment produced in the primary photodissociation step can be excited vibrationally and/or electronically,[26] and the departing H fragment can be scattered superelastically from the excited C_2H. However, even assuming that all of this excitation, which is about 0.5 eV at a maximum, would be transferred into the H-atom kinetic energy would not account for the faster fragments above ∼1.3 eV observed here. In addition, the argument that fast H fragments were observed even in Ar clusters with a single C_2H_2 molecule suggests that the contribution of this mechanism is not significant.

We did not observe a significant dependence of the photodissociation process on the cluster composition (mixed Ar/acetylene vs pure acetylene) or size (in the size range of 10−130); see Figure 5. This suggests that the above-proposed mechanism leading to the faster H fragments operates as soon as the C_2H_2 molecule is accompanied by a few solvent molecules. The KED in Figure 3c shows that this effect occurs already in $(C_2H_2)_n$ clusters with $\bar{n} \leq 10$.

In the above-discussed TOF spectra, we did not observe a strong zero-kinetic-energy peak, as was seen for the photodissociation of hydrogen halides in rare-gas clusters, for example, in ref 6. Such peaks, though less pronounced, are, however, observed in the spectra of C_2H_2 molecules picked up by the large Ar_n clusters in Figure 6. In this case, the H fragments from the C_2H_2 molecules should be produced by the same mechanism as proposed above; however, some of the fragments will be slowed by the cluster environment to near-zero kinetic energy before escaping. Therefore, an escaping H fragment will have to pass through Ar layers, where it can lose energy by inelastic collisions with Ar atoms. On the other hand, even in larger $(C_2H_2)_n$ clusters, the surface acetylene molecules are more likely to interact with the photons, and the fragments will escape from the near-surface C_2H_2 without too many inelastic collisions with the neighboring molecules.[39] The cluster is capable of quenching the dissociation started by the first photon for a significant fraction of molecules, even for the near-surface C_2H_2 molecules. Some hydrogens atoms, however, are able to leave the molecule. Once a hydrogen atom is produced in the dissociation, it soon leaves the cluster without a significant kinetic energy loss. The picture remains the same even after the second (or third, etc.) photon absorption. It is worth noting that, although zero-kinetic-energy fragments are unambiguously present in the TOF spectra, quantitatively, their contribution in the corresponding KEDs is negligible (see the discussion of Figure 6).

V. Conclusions

We have studied the photodissociation of $(C_2H_2)_n$ and $(C_2H_2)_n \cdot Ar_m$ molecular clusters prepared under various expansion conditions. Using mass spectrometric analysis, comparison with size-selective measurements of similar clusters, and model calculations, we determined the mean cluster sizes. In photodissociation experiments, we measured the H-fragment kinetic energy distribution spectra for these clusters.

The measured hydrogen KEDs of the acetylene clusters display features similar to those of the KED spectrum of the

isolated molecule; in particular, the KED maximum is located at approximately 0.2 eV for both isolated and solvated acetylene. However, the small fraction of zero energies and especially the long energy tail extending up to 2 eV are observed only for solvated acetylene. Whereas fragments with zero energies are a typical feature of the solvent cage effect, fragment acceleration upon solvation is atypical.

We analyzed the experiments from an energy perspective based on ab initio calculations. The following conclusions were made: (1) Under the present experimental conditions, multiphoton processes take place. (2) At 193 nm, the photodissociation is probably dominated by a singlet-state mechanism. (3) The solvent induces photostability of the acetylene molecule, and acetylene relaxes into a vibrationally hot ground electronic state. (4) The vibrationally excited molecule absorbs a subsequent photon and eventually dissociates, resulting in the faster fragments.

The scenario outlined above seems to be consistent with the static ab initio calculations and with all available experimental data. To ultimately confirm all of the reaction steps, it would be desirable to perform dynamic simulations. For such a small molecule as acetylene, this is, in principle, feasible.

Acknowledgment. This work was supported by the special program "Nanotechnology for Society" of the Czech Academy of Sciences via Grant KAN400400651 and Grant 203/09/0422 of the Grant Agency of the Czech Republic. P.S. also acknowledges postdoctoral Grant 203/07/P449 and computational support of the research center LC512, and M.F. acknowledges a special J. E. Purkyně fellowship of the Czech Academy of Sciences. I.D. acknowledges the DFG Research Training Group GRK 782 for supporting his stay in Prague. M.O. is a student of IMPRS' Dynamical Processes in Atoms, Molecules, and Solids.

Supporting Information Available: Cartesian coordinates of important points on the potential energy surface. This material is available free of charge via the Internet at http://pubs.acs.org.

References and Notes

(1) Franck, J.; Rabinovitsch, E. *Trans. Faraday Soc.* **1934**, *30*, 120.
(2) Alimi, R.; Gerber, R. B. *Phys. Rev. Lett.* **1990**, *64*, 1453.
(3) Gerber, R. B.; McCoy, A. B.; García-Vela, A. *Annu. Rev. Phys. Chem.* **1994**, *45*, 275.
(4) Baumfalk, R.; Buck, U.; Frischkorn, C.; Nahler, N. H.; Hüwel, L. *J. Chem. Phys.* **1999**, *111*, 2595.
(5) Buck, U. *J. Phys. Chem. A* **2002**, *106*, 10049.
(6) Fárník, M.; Nahler, N. H.; Buck, U.; Slavíček, P.; Jungwirth, P. *Chem. Phys.* **2005**, *315*, 161.
(7) Ončák, M.; Slavíček, P.; Poterya, V.; Fárník, M.; Buck, U. *J. Phys. Chem. A* **2008**, *112*, 5344.
(8) Poterya, V.; Fárník, M.; Slavíček, P.; Buck, U.; Kresin, V. V. *J. Chem. Phys.* **2007**, *126*, 071101.
(9) Poterya, V.; Fárník, M.; Ončák, M.; Slavíček, P. *Phys. Chem. Chem. Phys.* **2008**, *10*, 4835.
(10) Poterya, V.; Profant, V.; Fárník, M.; Slavíček, P.; Buck, U. *J. Chem. Phys.* **2007**, *127*, 064307.
(11) Poterya, V.; Votava, O.; Fárník, M.; Ončák, M.; Slavíček, P.; Buck, U.; Friedrich, B. *J. Chem. Phys.* **2008**, *128*, 104313.
(12) Gerber, R. B. *Annu. Rev. Phys. Chem.* **2004**, *55*, 55.
(13) Chastaing, D.; Underwood, J.; Wittig, C. *J. Chem. Phys.* **2003**, *119*, 928.
(14) Baumfalk, R.; Nahler, N. H.; Buck, U. *Phys. Chem. Chem. Phys.* **2001**, *3*, 2372.
(15) Cui, Q.; Morokuma, K.; Stanton, J. *Chem. Phys. Lett.* **1996**, *263*, 46.
(16) Cui, Q.; Morokuma, K. *Chem. Phys. Lett.* **1997**, *272*, 319.
(17) Malsch, K.; Rebentisch, R.; Swiderek, P.; Hohlneicher, G. *Theor. Chem. Acc.* **1998**, *100*, 171.
(18) Malsch, K.; Hohlneicher, G.; Schork, R.; Koppel, H. *Phys. Chem. Chem. Phys.* **2001**, *3*, 5393.
(19) Ventura, E.; Dallos, M.; Lischka, H. *J. Chem. Phys.* **2003**, *118*, 1702.
(20) Halasz, G.; Vibok, K.; Baer, M. *Chem. Phys. Lett.* **2005**, *413*, 226.
(21) Thom, R.; Wong, B.; Field, R.; Stanton, J. *J. Chem. Phys.* **2007**, *126*, 184307.
(22) Koppel, H.; Schubert, B.; Lischka, H. *Chem. Phys.* **2008**, *343*, 319.
(23) Mordaunt, D. H.; Ashfold, M. N. R. *J. Chem. Phys.* **1994**, *101*, 2630.
(24) Wodtke, A. M.; Lee, Y. T. *J. Phys. Chem.* **1985**, *89*, 4744.
(25) Fletcher, T. R.; Leone, S. R. *J. Chem. Phys.* **1989**, *90*, 871.
(26) Balko, B. A.; Zhang, J.; Lee, Y. T. *J. Chem. Phys.* **1991**, *94*, 7958.
(27) Zhang, J.; Riehn, C. W.; Dulligan, M.; Wittig, C. *J. Chem. Phys.* **1995**, *103*, 6815.
(28) Hsu, Y.-C.; Chen, F.-T.; Chou, L.-C.; Shiu, Y.-J. *J. Chem. Phys.* **1996**, *105*, 9153.
(29) Mordaunt, D. H.; Ashfold, M. N. R.; Dixon, R. N.; Löffler, P.; Schnieder, L.; Welge, K. H. *J. Chem. Phys.* **1998**, *108*, 519.
(30) Lauter, A.; Lee, K.; Jung, K.; Vatsa, R.; Mittal, J.; Volpp, H. *Chem. Phys. Lett.* **2002**, *358*, 314.
(31) Ganot, Y.; Golan, A.; Sheng, X.; Rosenwaks, S.; Bar, I. *Phys. Chem. Chem. Phys.* **2003**, *5*, 5399.
(32) Suzuki, T.; Hashimoto, N. *J. Chem. Phys.* **1999**, *110*, 2042–2050.
(33) Tsuji, K.; Terauchi, C.; Shibuya, K.; Tsuchiya, S. *Chem. Phys. Lett.* **1999**, *306*, 41.
(34) Yamakita, N.; Iwamoto, S.; Tsuchiya, S. *J. Phys. Chem. A* **2003**, *107* (15), 2597.
(35) Baumfalk, R.; Buck, U.; Frischkorn, C.; Gandhi, S. R.; Lauenstein, C. *Ber. Bunsen-Ges. Phys. Chem.* **1997**, *101*, 606.
(36) Slavíček, P.; Jungwirth, P.; Lewerenz, M.; Nahler, N. H.; Fárník, M.; Buck, U. *J. Chem. Phys.* **2004**, *120*, 4498.
(37) Werner, H.-J.; Knowles, P. J.; Lindh, R.; Manby, F. R.; Schütz, M.; Celani, P.; Korona, T.; Rauhut, G.; Amos, R. D.; Bernhardsson, A.; Berning, A.; Cooper, D. L.; Deegan, M. J. O.; Dobbyn, A. J.; Eckert, F.; Hampel, C.; Hetzer, G.; Lloyd, A. W.; McNicholas, S. J.; Meyer, W.; Mura, M. E.; Nicklass, A.; Palmieri, P.; Pitzer, R.; Schumann, U.; Stoll, H.; Stone, A. J.; Tarroni, R.; Thorsteinsson, T. *Molpro, A Package of Ab Initio Programs*, version 2006.1; University College Cardiff Consultants Limited: Cardiff, U.K., 2006.
(38) Bobbert, C.; Schütte, S.; Steinbach, C.; Buck, U. *Eur. Phys. J. D* **2002**, *19*, 183.
(39) Shuler, K.; Dykstra, C. E. *J. Phys. Chem. A* **2000**, *104*, 4562.
(40) Latajka, Z.; Scheiner, S. *Chem. Phys.* **1997**, *216*, 37.
(41) Baumfalk, R.; Nahler, N. H.; Buck, U.; Niv, M. Y.; Gerber, R. B. *J. Chem. Phys.* **2000**, *113*, 329.
(42) Hagena, O. F. *Surf. Sci.* **1981**, *106*, 101.
(43) Chickos, J. S.; Acree, W. E. *J. Phys. Chem. Ref. Data* **2002**, *31*, 537–698.
(44) From the absorption cross section for a C_2H_2 molecule of $\sigma = 1.347 \times 10^{-19}$ cm^{-2},[45] it would follow that about 50 photons could be absorbed by the molecule within the 25-ns laser pulse, provided that the molecule absorption cross section does not change after photon absorption. Alternatively, up to about 50 molecules could be dissociated in the cluster within the laser pulse.
(45) Seki, K.; Okabe, H. *J. Phys. Chem.* **1993**, *97*, 5284.
(46) The detection probability is a steep function of the fragment kinetic energy: The zero-kinetic-energy fragments are accelerated by the weak extraction field directly into the detector and detected with almost 100% efficiency, whereas the faster fragments with a velocity component perpendicular to the WMTOF axis can escape detection. This detection probability is taken into account by the MC simulations in the TOF → KED conversion procedure. Therefore, even a strong zero-kinetic-energy peak in the TOF spectrum is suppressed substantially by the transformation to the KED. The KEDs corresponding to the present TOF spectra are very similar, with only minor differences in the near-zero region despite the different zero-kinetic-energy peaks in the TOF spectra.
(47) Even at the highest laser powers corresponding to photon fluxes of 10^{28} cm^{-2} s^{-1}, the time delay between two consecutive photons hitting a C_2H_2 molecule is, on average, about 0.5 ns (assuming a molecular absorption cross section of $\sigma = 1.347 \times 10^{-19}$ cm^{-2} [45]). For comparison, the photodissociation process at 193 nm occurs on a timescale of approximately 100 ps.[34]
(48) Lipciuc, M.; Wang, F.; Yang, X.; Kitsopoulos, T.; Fanourgakis, G.; Xantheas, S. *Chem. Phys. Chem.* **2008**, *9*, 1838.
(49) Miller, R. E. *Science* **1988**, *240*, 447.
(50) Zhong, Q.; Castleman, A. W. *Chem. Rev.* **2000**, *100*, 4039.
(51) Dermota, T. E.; Zhong, Q.; Castleman, A. W. *Chem. Rev.* **2004**, *104*, 1861.

JP811073J